crystals

MDPI

Article

The Rigidity of the (BH_4)-Anion Dispersed in Halides AX, A = Na, K; X = Cl, Br, I, and in MBH_4 with M = Na, K, Rb, Cs

Zeina Assi [1], Alexander Gareth Schneider [2], Anna Christina Ulpe [2], Thomas Bredow [2] and Claus Henning Rüscher [1,*]

[1] Institut für Mineralogie, Leibniz Universität Hannover, Callinstr. 3, D-30167 Hannover, Germany; zeina.assi@hotmail.de

[2] Mulliken Center for Theoretical Chemistry, Rheinische Friedrich-Wilhelm-Universität Bonn, Bergstr. 4-6, D-53115 Bonn, Germany; alexander.schneider@dguv.de (A.G.S.); anna@thch.uni-bonn.de (A.C.U.); bredow@thch.uni-bonn.de (T.B.)

* Correspondence: c.ruescher@mineralogie.uni-hannover.de

Abstract: The B–H bond length of the borohydride anion (BH_4^-) in alkali metal borohydrides MBH_4 with M = Na, K, Rb, Cs, and diluted in different alkali halide matrices, was investigated experimentally by infrared spectroscopy (FTIR) and theoretically using first principles calculations. The peak positions in IR absorption spectra of $NaBH_4$ pressed at 754 MPa in halides NaX and KX with X = Cl, Br, I show significant variations indicating ion exchange effects between the halide and $NaBH_4$. For $NaBH_4$ in NaBr, NaI, KBr and KI pellets, the peak positions indicate that BH_4^- could be highly diluted in the AX matrix, which renders an isolation of BH_4^- in AX (i-BH_4^-). For $NaBH_4$ in NaCl and KCl pellets, a solution of BH_4^- in AX occurred only after a further thermal treatment up to 450 °C. The observed peak positions are discussed with respect to the lattice parameter (a_0), anion to cation ratio ($R = r_A/r_X$), standard enthalpy of formation ($\Delta_f H$) and ionic character (I_c) of the halides. A linear relation is obtained between ν_3(i-BH_4^-) and the short-range lattice energies of AX. Density functional theory (DFT) calculations at generalized gradient approximation (GGA) level were used to calculate the IR vibrational frequencies ν_4, ν_3 and $\nu_2 + \nu_4$ for series of compositions $Na(BH_4)_{0.25}X_{0.75}$ with X = Cl, Br, I, and MBH_4. The theoretical and experimental results show the same trends, indicating the rigidity of the B–H bond length and the failure of Badger's rule.

Keywords: alkali metal borohydride; BH_4^- in halide; infrared spectroscopy; first principle calculations

Citation: Assi, Z.; Schneider, A.G.; Ulpe, A.C.; Bredow, T.; Rüscher, C.H. The Rigidity of the (BH_4)-Anion Dispersed in Halides AX, A = Na, K; X = Cl, Br, I, and in MBH_4 with M = Na, K, Rb, Cs. *Crystals* **2022**, *12*, 510. https://doi.org/10.3390/cryst12040510

Academic Editor: Sergio Brutti

Received: 9 March 2022
Accepted: 1 April 2022
Published: 6 April 2022

1. Introduction

Borohydrides, conventionally called tetrahydroborates following the recommendation of the International Union of Pure and Applied Chemistry (IUPAC), have received attention due to their remarkable gravimetric and volumetric hydrogen contents [1]. Here, the anionic part is constituted of the tetrahedral BH_4^- group and the negative charge on the borohydride unit is generally compensated by alkali or alkaline earth metals. This has been known since the discovery of $NaBH_4$ and moreover their potential use as reducing agents [2]. Alkaline solutions of $NaBH_4$ were already used for producing electrical energy with fuel cell technology in Apollo missions. However, a breakthrough for a viable hydrogen economy is not achieved because of the irreversibility of the hydrogen release, although there were great efforts for better understanding the related problems and also receiving technical solutions for suitable applications of using $NaBH_4$ as hydrogen storage [3].

Fundamental research shows that the thermal desorption of H_2 occurs at temperatures above 450 °C and leads to a decomposition of the compound into the elements according to $MBH_4 \Rightarrow M + B + 2H_2$ [1,4]. Some novel approaches could reduce the hydrogen desorption temperature including catalysis [5,6], nano-engineering [7,8] and use of reactive additives [9–11]. Some work includes the enclosure and handling of the BH_4^- anion in sodalite cages [12,13], or $NaBH_4$ in an aluminosilicate gel [13,14]. The investigations of the

BH_4^- anion in the sodalite cages were mainly focused on the thermal control of steps of the effective reaction:

$$BH4^- + 2H_2O = > BO_2^- + 4H_2, \quad (1)$$

Reaction (1) is supported by previous investigations showing that half of the released hydrogen is supplied by water [3]. In a combined theoretical and experimental approach [15], $B(OH)_3/(OH)^-$, $B(OH)_4^-$ and $BO(OH)_2^-$ could be identified as intermediates in the sodalite cages finally receiving BO_2^-. In a more recent investigation [16], it was concluded that an initial reaction reveal (BH_3) and $(OH)^-$ in separated sodalite cages followed by a fast reaction:

$$BH_3 + 3H_2O = > B(OH)_3 + 3H_2, \quad (2)$$

Thus, the reaction sequence could be in close analogy to conclusions by Mesmer and Jolly [17] that hydrolysis of $NaBH_4$ in aqueous solutions take place forming initially BH_5 which separates into $BH_3 + H_2$. Kreevoy and Hutchins [18] attributed it to an acid catalyzed mechanism, where BH_3 rather rapidly reacts with $3H_2O$ to $B(OH)_3$ plus $3H_2$, and $B(OH)_3$ reacts successively with $(OH)^-$ to $B(OH)_4^-$.

Basic questions still concern details of the stability of the BH_4^- anion in various borohydrides. Nakamori et al. [19,20] reported a correlation between the first hydrogen desorption temperature (T_d) of the metal borohydrides and the Pauling electronegativity (χ_P) of the metal cations, while T_d decreases with increasing χ_P of the metal. An apparent linear relationship was obtained between the T_d and χ_P for the borohydrides of Na, Li, Mg, Sc, Zr and Zn indicating that χ_P could be considered as an indicator for approximate estimations of the stability of borohydrides. This relation is applicable for other classes of hydrides as tetra-alanates (AlH_4^-) [21] and hexa-alanates (AlH_6^{3-}) [22], too. Hence, one approach to affect the thermal stability of metal borohydrides is to introduce a metal with higher electronegativity through lattice cation substitution. For example, for the cation substitution of Na ($\chi_P = 0.93$), (The χ_P values are dimensionless and are given according to Pauling's scale for the elements of the periodic table; χ_P is defined as the power of an atom in a molecule to attract electrons [23]) and Li ($\chi_P = 0.98$) with Zn ($\chi_P = 1.65$) in $NaBH_4$ and $LiBH_4$ salts, respectively, by mechanically ball milling the borohydride salts with $ZnCl_2$ produces mixed-metal of borohydrides $NaZn(BH_4)_3$, $NaZn_2(BH_4)_5$ and $LiZn_2(BH_4)_5$, which are thermally less stable than their unsubstituted patterns [24].

The anion substitution in the alkali metal borohydride is also used to tune the thermodynamics of the borohydrides. The mixed hydride-fluoride $Na_3AlH_{(6-x)}F_x$ prepared from NaF, Al and H_2 is destabilized relative to the pure hydride Na_3AlH_6 [25]. Likewise, first-principles calculations of the decomposition reaction of $LiBH_4$ with and without fluorine F^- suggested that doping $LiBH_4$ with F^- results in a partial substitution of H by F in the hydride lattice yielding favorable thermodynamics modifications [26]. In a more recent study on ball milled samples of $NaBH_4$ and $NaBF_4$, the authors reported a fluorine substitution in the temperature range 200–215 °C yielding $NaBH_2F_2$. The $NaBH_4$-$NaBF_4$ composite decomposes at temperatures by at least 100 °C lower in comparison with $NaBH_4$ [10].

The anion substitution may involve the whole borohydride unit as the substitution of BH_4^- by Cl^- in $NaBH_4$ [27,28], and with Br^- [29] and I^- [30] in $LiBH_4$, respectively. Differential Scanning Calorimetry (DSC) measurements of the solid solutions reveal the endothermic peaks of the melt as an indicator of the thermal stability at higher temperatures compared to the unsubstituted borohydride salts, suggesting that hydrogen release is not improved by these substitutions.

The stabilization/destabilization effect upon the lattice substitutions could be attributed to the different types of interactions altered during the ionic exchange. The ionic bonding is effective between the cation element and the BH_4^- group, whereas the bonding between the boron B and the hydrogen H atoms within the BH_4^- group shows a covalent character [31]. The present work is focused on a better understanding of the interactions between the BH_4^- anion and its environment. Room temperature, Raman and infrared

spectroscopic studies of alkali borohydrides MBH_4, M = Na, K, Rb and Cs, could be fully assigned by Renaudin et al. [32] for both hydrides and deuterides, including the overtones with Fermi resonance and combination bands of the BH_4^- anion, which was in agreement with previous assignments [33–36]. The data were found to be in perfect agreement with Badger's rule possessing a linear relationship between vibrational frequencies and the B–D bond length. We show here that for the BH_4^- anion highly diluted in halide matrices AX, A = Na, K; X = Cl, Br, I, a simple space argument does not consistently predict extension or contraction of B–H bond distances. Instead, details of the effective potential function are found to be more important. First principles calculations support the conclusion that there are only rather small changes in B–H bond distances although there are large variations in lattice parameter dependent on composition.

2. Materials and Methods

2.1. Experimental Study of BH_4^- Anion Isolated in AX Halides

Commercial samples of sodium borohydride $NaBH_4$ (Merck, ≥98%), potassium borohydride (53.94 g·mol^{-1}, Aldrich, 99.9%), sodium chloride NaCl (Merck, ≥9.5%), sodium bromide NaBr (Fluka, ≥99.0%), sodium iodide NaI (Fluka, ≥99.0%), potassium chloride KCl (Merck, ≥99.5%), potassium bromide KBr (Roth) and potassium iodide KI (Riedel-de Haën, 99–100.5%) were used in this study.

Attenuated total reflectance FTIR-ATR spectra of as-received $NaBH_4$ and KBH_4 samples were recorded on the Bruker ifs 66 v/S using an ATR accessory with a diamond crystal. The vibrational spectra of borohydrides can be divided into two regions: the bond bending region (with ν_2 and ν_4, the symmetric and asymmetric bending modes, respectively) from 1050 to 1300 cm^{-1} and the bond stretching region (with ν_1 and ν_3, the symmetric and asymmetric stretching modes, respectively) from 2100 to 2500 cm^{-1} [32]. The asymmetric modes ν_4 and ν_3 are IR active. The B–H bond bending vibrations occur at about half the bond stretching vibrations implying overtone ($2\nu_4$) and combination ($\nu_2 + \nu_4$) with Fermi resonance [35,36].

MBH_4/AX pellets (M = Na and K) of 13 mm diameter were produced by exerting a force of 100 kN (equivalent to a pressure of 754 MPa) on a mixture consisting approximately of 0.5 wt% MBH_4 and 99.5 wt% AX for one minute. Fourier transform infrared (FTIR) spectra of $NaBH_4$ diluted in different halide matrices were taken using the Bruker Vertex 80 v FTIR spectrometer under vacuum. $NaBH_4$/NaCl and $NaBH_4$/KCl pellets were further heated under vacuum to 450 °C. IR spectra after the thermal treatment were recorded on the Bruker ifs 66 v/S FTIR spectrometer.

2.2. First Principles Calculations

All calculations were performed with the crystalline orbital program CRYSTAL14 [37,38]. All parameters and functionals were tested in a previous work [15]. We used the PWGGA [39] functional, CRYSTAL standard basis sets for sodium, potassium, boron, hydrogen and chlorine, a TZVP basis set for bromine with an additional f-function and pseudopotential basis sets for rubidium, cesium and iodine (Table 1).

The truncation criteria in all calculations for bielectronic integrals were set to 10^{-9} (overlap and penetration threshold for Coulomb-integrals, overlap threshold for exchange-integrals, pseudo-overlap) and 10^{-18} (pseudo-overlap), respectively. The SCF (self-consistent-field) convergence threshold on total energy was set to 10^{-7} a.u. for geometry optimizations and to 10^{-10} a.u. for frequency calculations, respectively. A *Monkhorst-Pack*-net of 8 × 8 × 8 was employed and a maximum trust radius of 0.3 *Bohr* was used in the optimizations. The Anderson method for accelerating convergence was used.

Table 1. Atomic basis sets used in the CRYSTAL calculations.

Atom	Basis Set
Na	8-511G [40]
K	86-511G [40]
Rb	ECP28MWB [41]
Cs	ECP46MWB [41]
H	5-11G * [42]
B	6-21G * [43]
Cl	86-311G [44]
Br	Pob-TZVP [45]
I	ECP [46]

* related to the nomenclature of the basis set.

We used the experimental structures [32,47] as a starting point and fixed the lattice constants in the geometry optimizations, but not the atomic positions. Due to the computational afford, we calculated no supercells for dilution of BH_4^- in metal halides but unit cells with one BH_4^- and three halides, which is a ratio of 25% of BH_4^-. The frequencies were calculated with fully optimized atomic positions. The antisymmetric stretching mode was enharmonically corrected [15]. The calculated modes were visualized with the program Jmol [48] and could thereby be assigned to the different mode types.

3. Results and Discussion

3.1. Spectra of $NaBH_4$/KBH_4 in ATR and Pressed in Various Halides

The ATR spectra of as-received $NaBH_4$ and KBH_4 powders are shown in Figure 1. The positions of the peak maxima are in good agreement with values reported by Renaudin et al. [32] as collected in Table 2 together with the assignment given. It is well known that the bands in the ATR spectra are generally shifted to lower frequencies compared to the transmission spectra due to the dispersion of the refractive index. This is one reason that the IR peak positions obtained using the standard pressed pellet technique, e.g., in KBr halide shows deviations from peak positions determined using ATR.

Table 2. ATR frequencies of $NaBH_4$ and KBH_4 compared to ATR values of Renaudin et al. [32] (values in brackets) in addition to the transmission IR frequencies of $NaBH_4$ in KBr and NaCl pellets.

		ν_4	$2\nu_4$	ν_3	$\nu_2 + \nu_4$
ATR	NaBH4	1110 (1110)	2217 (2217)	2283 (2284)	2397 (2404)
	KBH_4	1111 (1112)	2205 (2208)	2268 (2270)	2375 (2376)
Transmission (pellets)	$NaBH_4$/NaCl	1121	2229	2302	2403
	$NaBH_4$/KBr (<30 s pressed)	1120	2220	2299	2398
	$NaBH_4$/KBr (90 s pressed)	1126	2224	2291	2387

Another reason for deviations in the peak positions determined in the pressed pellet method is related to a rather uncontrolled anion or cation exchange effect between the probe and the matrix. This is shown in Figure 2 for $NaBH_4$ in KBr (spectrum b, c). Rather broad and less well-determined peak positions are observed for short mixing and pressing time (30 s, spectrum b). At variance, good mixing and 90 s pressing at the same force (100 kN/13 mm diameter sample = 754 MPa) reveal much sharper and shifted peak positions (spectrum c). The positions of the peak maxima are also given in Table 2 for comparison. The better mixing and longer pressing time obviously leads to better resolved peaks, e.g., for the isotope effect $^{11}B/^{10}B$ depicted by the shoulder at higher wavenumbers seen for ν_4 and $2\nu_4$. This better resolution is explained, however, by a higher degree of solution of the BH_4^- anion into the KBr matrix. In this respect, the broader peaks seem

to be more representative for $NaBH_4$. This is supported by inspection of the spectrum obtained for $NaBH_4$ diluted and pressed into NaCl also shown in Figure 2 (spectrum a). The peaks well coincide with those of $NaBH_4$ in KBr also taken from the typically broader one. Spectra given for $NaBH_4$ in NaBr (d) and KI (e) also show rather sharp peaks but at significant different peak positions. This indicates the effect of a sufficient dilution and incorporation of the BH_4^- anion in the various metal halide type lattices.

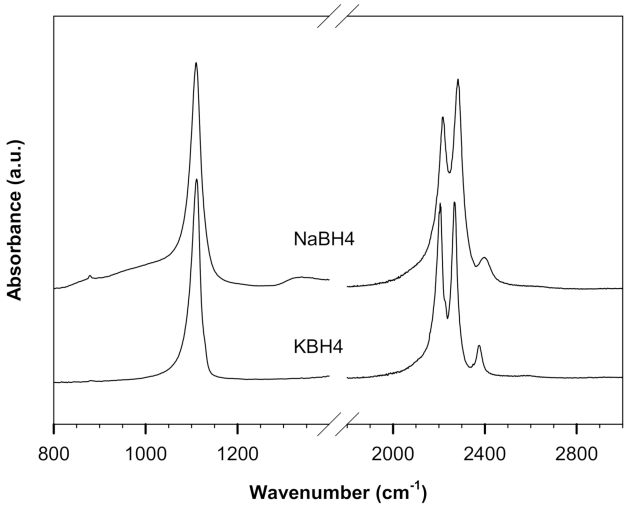

Figure 1. FTIR−ATR spectra of the as-received $NaBH_4$ and KBH_4 samples.

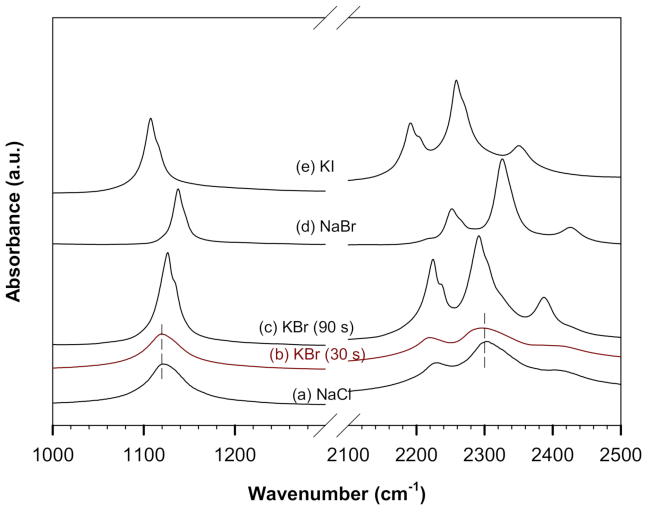

Figure 2. Room temperature transmission IR spectra of as−received $NaBH_4$ in NaCl (**a**), in KBr short pressed (**b**) and long pressed (**c**), in NaBr (**d**) and in KI (**e**). Vertical dashed lines are used to show the coincidence of peak positions of ν_4 and ν_3 of (**a**,**b**).

It has been reported that the BH_4^- anions are highly diluted in AX by heating discs constituted of AX and traces of borohydride ($NaBH_4$ or KBH_4) to temperatures between 500 and 600 °C [49]. For our purpose, this effect is demonstrated in Figure 3. Shown are spectra for $NaBH_4$ (1 mg) diluted into 200 mg of NaCl and KCl (dashed curves) compared to those after heating to 450 °C (red solid lines). For $NaBH_4$ in NaCl after the thermal treatment, the IR peaks appeared to be sharpened and shifted to higher wavenumbers compared to spectra taken before the heating. For $NaBH_4$ diluted and pressed with KCl, the spectrum shows peak splitting indicating the formation of two types of solid solution with a higher and smaller BH_4^- anion concentration in KCl. However, after thermal treatment, a more homogeneous dilution of BH_4^- anions in KCl crystals is obtained.

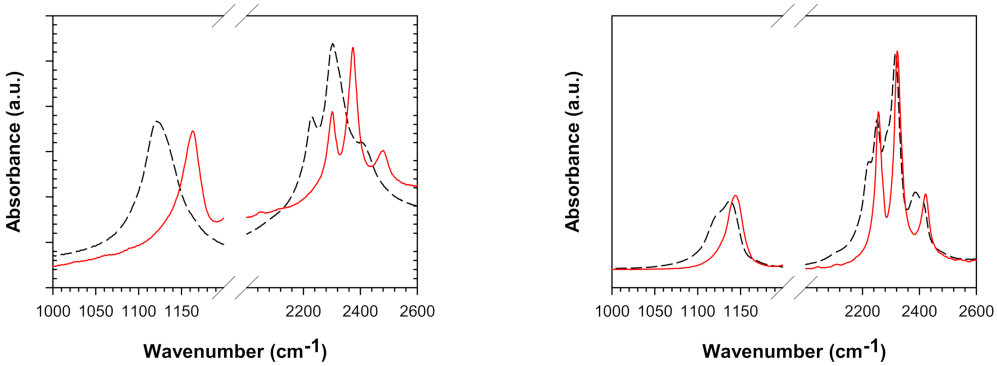

Figure 3. IR spectra of $NaBH_4$ diluted in (**a**) NaCl and (**b**) KCl pellets before (black dashed lines) and after thermal treatment to 450 °C (red solid lines).

3.2. BH_4-Frequency Variations Dependences on Halide Parameters

The pellet preparation procedure using a pressure of approximately 754 MPa was sufficient to solve $NaBH_4$ (a_0 = 6.16 Å) in NaI (a_0 = 6.48 Å), NaBr (a_0 = 5.97 Å), KBr (a_0 = 6.60 Å) and KI (a_0 = 7.06 Å), whereas for NaCl (a_0= 5.64 Å) and KCl (a_0 = 6.29 Å), a subsequent annealing to 450 °C was required to achieve the total solution of BH_4^- in the halide lattice. This can be related to the smaller effective ionic radius of Cl^- (1.80 Å [28]) compared to BH_4^- (2.03 Å [29]). On the other hand, the ionic radii of Br^- (1.96 Å [29]) and I^- (2.20 Å [30]) are close or significantly larger, respectively. Therefore, a much better exchange is already achieved by the pressure effect. The larger cation radius of K^+ compared to Na^+ may enhance the solution effect as could be suggested from the two type of compositions indicated in the $NaBH_4$ spectrum in KCl compared to $NaBH_4$ in NaCl (Figure 3).

The obtained IR frequencies of BH_4^- in different halide matrices in presumably the high dilution limit, denominated as i-BH_4^- (i for isolated) in the following, are summarized in Table 3 and compared to previous works [49,50]. The IR values for BH_4^- in RbX matrices are taken from ref. [50]. The cell parameter (a_0) [47] and the radius ratio of the effective ionic radius (NaCl structure, coordination number 6) of the cation to the ionic radius of the anion ($R = r_A/r_X$) [51] are also given in Table 3.

Table 3. IR frequencies of i-BH_4^- in different AX. Structural parameters of AX are also given.

AX	IR Frequencies of i-BH_4^- in AX				Structural Parameters of AX	
	ν_4	$2\nu_4$	ν_3	$\nu_2 + \nu_4$	a_0	$R = r_A/r_X$
NaCl	1165 1166 * 1167 **	2303 2307 * 2311 **	2375 2373 * 2382 **	2482 2486 * 2493 **	5.6402	0.5635
NaBr	1138 1136 * 1135 **	2252 2254 * 2257 **	2326 2328 * 2331 **	2426 2427 * 2430 **	5.9738	0.5204
NaI	1112 1111 *	2208 2202 *	2281 2278 *	2364	6.479	0.4636
KCl	1144 1144 * 1146 **	2257 2257 * 2262 **	2323 2324 * 2328 **	2422 2422 * 2428 **	6.290	0.7624
KBr	1127 1128 * 1128 **	2226 2226 * 2229 **	2293 2293 * 2295 **	2390 2387 * 2391 **	6.598	0.7041
KI	1107 1108 * 1108 **	2191 2191 * 2192 **	2258 2258 * 2258 **	2350 2341 * 2350 **	7.064	0.6273
RbCl	1132 **	2236 **	2303 **	2395 **	6.582	0.8398
RbBr	1118 **	2212 **	2279 **	2369 **	6.8768	0.7755
RbI	1104 **	2181 **	2250 **	2335 **	7.3291	0.6909

* IR values according to ref. [49]. ** IR values according to ref. [50].

It is observed that ν_3(i-BH_4^-) is similar in NaI and RbBr, 2281 and 2279 cm^{-1}, respectively, while the corresponding a_0 (6.479 Å and 6.877 Å, respectively) and ion radius ratio R (0.4636 and 0.7755, respectively) of the halide matrices are very different. Therefore, the frequencies of ν_3(i-BH_4^-) cannot be interpreted in terms of only the lattice parameter a_0 or R determining the available space for the substituting BH_4^- in AX. At variance, the IR frequencies of i-BH_4^- are dependent on the nature of the host matrix, as suggested in previous works for many polyatomic ions isolated in halide matrices [30,50]. To show this effect more clearly, graphical representations of ν_3(i-BH_4^-) as a function of the structural parameters, a_0 and R of the corresponding AX, are given in Figure 4a,b, respectively.

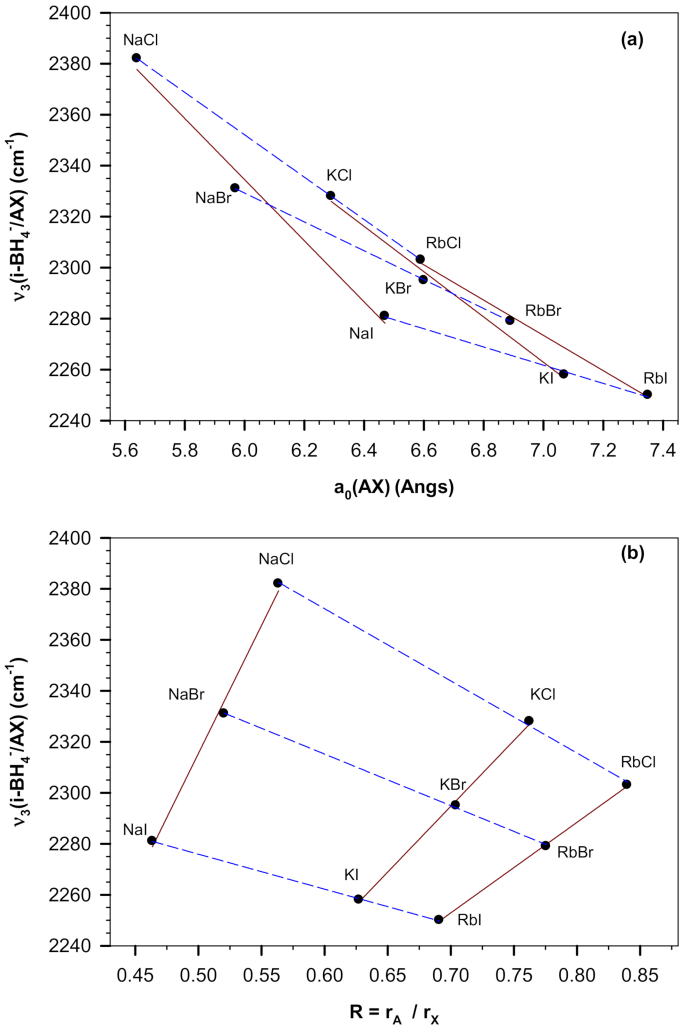

Figure 4. Graphical representation of ν_3(i−BH_4^-) as a function of (**a**) the cell parameter a_0 and (**b**) the radius ratio ($R = r_A/r_X$) of the corresponding AX halide. Red solid lines represent common cations (A-series) and blue dashed lines are for the common anion X-series.

Approximately, linear relationships are observed between ν_3(i-BH_4^-) and a_0(AX) for the homologous series of halides with same cationic element A (A-series, solid red lines) or with the same anionic element X (X-series, dashed blue lines). The linearity between ν_3(i-BH_4^-) and a_0(AX) applies within each of the defined series implying a decrease of ν_3(i-BH_4^-) with increasing a_0(AX) (Figure 4a). Furthermore, according to Figure 4b, an increase of ν_3(i-BH_4^-) is accompanied with an increase of R for the A-series (for a given A-series r_A is constant while r_X is decreasing) but with a decrease of R for the X-series (for a given X-series r_A is increasing while r_X is maintained constant). This indicates that ν_3(i-BH_4^-) varies in an opposite direction to the ionic radii of the cations (r_A) and the

anions (r_X). Smaller cations and anions tend to increase ν_3(i-BH_4^-). In other words, cations and anions of higher Pauling electronegativity (χ_P) within the A- or X-series exhibit higher ν_3(i-BH_4^-) since χ_P varies in an opposite direction to that observed for the ionic radius in the periodic table (χ_P increases by going from left to right across a period, and decreases by moving down a group). This still could indicate that increasing the available space for the substituting BH_4^- anion along a given A-series with increasing anion size (for e.g., NaCl, NaBr and NaI) decreases ν_3 by increasing the B–H distances. A similar effect occurs with increasing the size of the cation along a given X-series (for e.g., NaI, KI and RbI), an elongation of the B–H distances could be responsible of the decrease of ν_3(i-BH_4^-). This explanation fails, however, between different series as alluded above for the case of NaI and RbBr which exhibit similar ν_3(i-BH_4^-) but completely different available anion spaces. The same holds for NaBr and KCl matrices. Therefore, the main factor responsible of frequency variations is not based on the B–H bond distance considerations in these cases.

The linear relationship established between ν_3(i-BH_4^-) and a0(AX) can be presented empirically according to:

$$\nu_3(\text{i-}BH_4^-) = \alpha.a_0(AX) + \beta, \quad (3)$$

α is the gradient and β a constant obtained from the linear regressions and given in Table 4. The R^2 values (>0.98) are satisfactory and confirm the effectiveness of the correlations.

Table 4. Empirical constants (α and β) of the linear relationship ν_3(i-BH_4^-) = $\alpha.a_0$(AX) + β for common cation A- series and common anion X-series.

A-Groups	α (cm^{-1} Å^{-1})	β (cm^{-1})	R^2
Na-group	−119.9275	3054.0962	0.9848
K-group	−88.8481	2884.8024	0.9928
Rb-group	−69.1765	2757.6490	0.9956
X-groups			
Cl-group	−83.1449	2850.9477	0.9999
Br-group	−56.6220	2668.9545	0.9999
I-group	−35.7190	2511.7233	0.9957

The absolute value of α of the A-series decreases when descending group 1 of the periodic table, i.e., in the order Na-series > K-series > Rb-series. Similarly, the absolute values of α of the X-series decrease in the order Cl-series > Br-series > I-series. Assuming that the gradient α of the linear regression gives insight into the rate at which changes are taking place, i.e., how much the variations of a_0(AX) would affect the values of ν_3(i-BH_4^-), obtained results suggest that the dependency of ν_3(i-BH_4^-) on a_0(AX) diminishes across group 1 and group 17 of the periodic table, i.e., when increasing r_A of A-series and r_X of X-series, respectively. Furthermore, the absolute values of α of A-series are greater than those of the X-series. Since in a given A-series, the anionic element is varying and for a given X-series, the cationic element is changing; the obtained results suggest that the anionic element X of AX has more impact on ν_3(i-BH_4^-) than the cationic element A.

The interrelations established between ν_3(i-BH_4^-), a_0(AX) and R(AX) can be extended and discussed in term of other parameters of AX as the negative value of the standard enthalpy of formation (Δ_fH, or exothermicity = $-\Delta_f$H), the fractional ionic character of the bond for AX (I_c) and the electronegativity χ_P of A and X, respectively. It has been reported that -Δ_fH increase with increase of I_c of AX. Moreover, both parameters increase when R increases within a given A-series (r_X is changing) or X-series (r_A is changing) with the increase being deeper for A-series [51]. By combining these correlations with those deduced from Figure 4, it can be deduced that for the same cationic A-series, ν_3(i-BH_4^-) is positively correlated to -Δ_fH and I_c of AX, i.e., an increase of ν_3(i-BH_4^-) is accompanied with an increase of -Δ_fH and I_c of AX, respectively (Figure 5). For the homologous series with the same anionic element, an inverse correlation lies between ν_3(i-BH_4^-) and -Δ_fH

and I_c of AX, i.e., an increase of ν_3(i-BH_4^-) is accompanied with a decrease of -Δ_fH and I_c of AX, respectively.

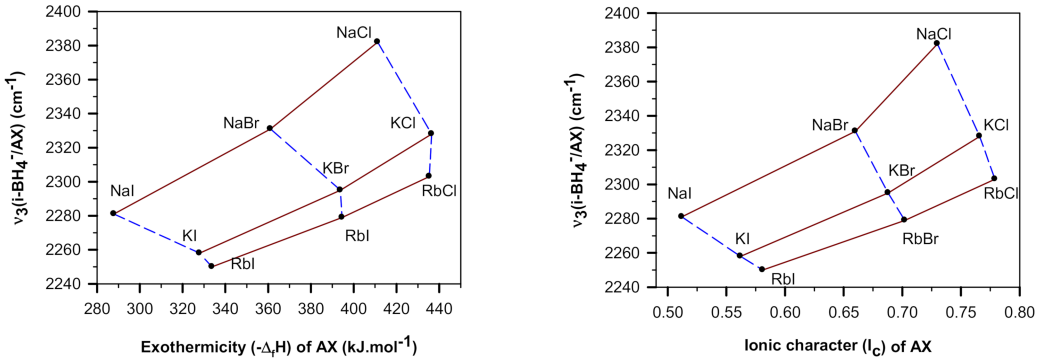

Figure 5. Graphical representation of ν_3(i$-BH_4^-$) in function of (**a**) the exothermicity ($-\Delta_f$H) of AX and (**b**) the ionic character (I_c) of the bond for AX halides. Red solid lines are for A−series and blue dashed lines are for X−series.

BH_4^- anion isolated in AX replaces the anion X^- at individual sites in the alkali halide lattice. Several complex empirical functions have been developed to carry out a quantitative evaluation of the frequencies shift of an isolated ion in different surroundings. In a general way, the potential function (V′) governing the vibration of a molecular ion substituted in NaCl-type cube can be regarded as the sum of the potential function of the free ion (V_F) and the interaction energy (V) arising from the presence of the environment expressed in terms of the interaction energy (U) (Equation (4)) [52].

$$V' = V_F + V, \tag{4}$$

The perturbing potential function (V, expressed in terms of the interaction energy) has two distinct effects on the considered ion: (i) the second derivatives of the perturbing potential with respect to appropriate symmetry coordinates which represent additional contributions to the effective force constants of the impurity ion and (ii) the first derivatives of the perturbing potential represent forces which modify the equilibrium internuclear spacing within the ion [52]. Accordingly, the frequency shift of the *i*th normal mode of the solute is given by:

$$\frac{\Delta \nu i}{\nu i} = \frac{1}{2ki}\left(\frac{\partial^2 V}{\partial S_i^2} - \frac{3a_{iii}}{a_{ii}}\frac{\partial V}{\partial S_i} - \sum_r \frac{a_{iir}}{a_{rr}}\frac{\partial V}{\partial S_r}\right), \tag{5}$$

where *ki* is the force constant of the *i*th mode, *Si* are the normal co-ordinates and *a* are the potential constants [53]. For a diatomic ion described by a Morse potential of the form $V_F = D\left(1 - e^{-\beta\xi}\right)^2$ the equation is reduced to:

$$\frac{\Delta \nu}{\nu} = \frac{1}{2k}\left(\frac{\partial^2 V}{\partial \xi^2} + 3\beta\frac{\partial V}{\partial \xi}\right), \tag{6}$$

where $\xi = r - r_e$ is the change in the internuclear spacing [53,54]. The perturbing potential can be explicitly expressed based on the classical theory of ionic crystals given by Born and Mayer as the sum of a polarization term (V_p) arising from static or dynamic polarization of the isolated ion or the surrounding lattice, a columbic term (V_c) describing the charge–charge interaction between the solute ion and the supporting alkali halide lattice and a repulsive short-range term (V_s) due to the overlap of electron density of the isolated ion with its surrounding ions of the lattice [52,54]. In most cases where the terms of Equation (4) or its equivalent have been evaluated, it was found that the first derivative

term (force multiplied by anharmonicity) dominated the frequency shift calculations [53]. For example, for the cyanide ion CN^- isolated in various alkali halides [54], the authors observed that the frequency shifts calculations are sensitive to very small changes in the position of the nearest neighbor ions and are dominated by the repulsive term shortening of the CN bond.

An approximately linear relation is obtained between ν_3(i-BH_4^-) and the short-range lattice energies of AX (Figure 6). The short lattice energy of AX can be considered as the contribution of the repulsive, dipole–dipole and dipole–quadrupole interaction energies given by the Born–Mayer equation AX. These values are tabulated in Table 5 and make clear evidence that the repulsive forces constitute the major part. Similar linear correlation was reported for the nitrate anion NO_3^- embedded in different halide matrices [55]. We also obtained the same linear dependency for CN^- in different halides basing on the IR frequencies of reference [54].

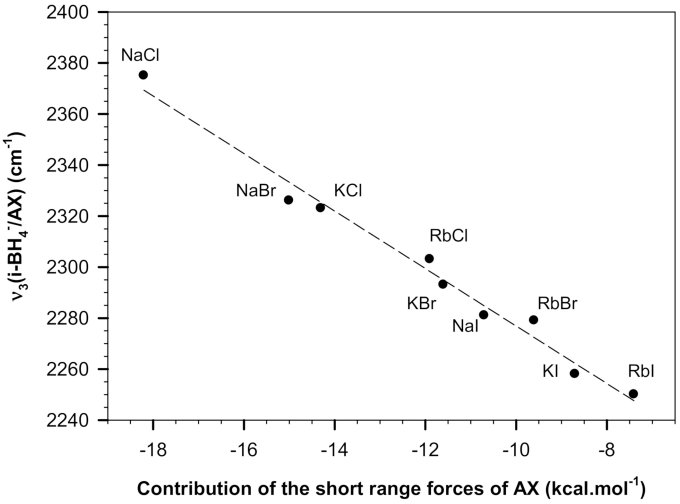

Figure 6. Graphical representation of ν_3(i$-BH_4^-$) as a function of the contribution of the short-range interaction energies in the corresponding AX. Dashed line is the linear regression.

Table 5. Contribution of the short-range forces of the alkali halides as given by the Born–Mayer equation (in kg.cal.mol^{-1} [56]).

AX	Repulsive	Dipole-Dipole	Dipole-Quadrupole	Short Range
NaCl	−23.5	5.2	0.1	−18.2
NaBr	−20.6	5.5	0.1	−15
NaI	−17.1	6.3	0.1	−10.7
KCl	−21.5	7.1	0.1	−14.3
KBr	−18.6	6.9	0.1	−11.6
KI	−15.9	7.1	0.1	−8.7
RbCl	−19.9	7.9	0.1	−11.9
RbBr	−17.6	7.9	0.1	−9.6
RbI	−15.4	7.9	0.1	−7.4

The correlations between ν_3(i-BH_4^-) and χ_P(A) and χ_P(X) already discussed for the different series, can provide information about the stability of the borohydrides. Cations and anions of higher χ_P within the A- or X-series exhibit higher ν_3(i-BH_4^-). A more pronounced charge transfer to BH_4^- anion results in stronger B–H bonds stabilizing the borohydride [1]. A more electronegative cation destabilizes the borohydride by attracting the electron density and reducing the electron density in the B–H bonds [19]. For MBH_4 salts, the thermal stability increases in the order $NaBH_4$ < KBH_4 < $RbBH_4$ < $CsBH_4$ [57], whereas the χ_P of the cation increases in the opposite way. Orimo et al. [57] found that for lithium, sodium and potassium borohydrides, the Raman active stretching ν_1 and bending

ν_2 modes decrease in the order (ν_2 ($LiBH_4$) = 1295 cm^{-1} and $\nu_{2'}$ ($LiBH_4$) = 1305 cm^{-1}) > (ν_2 ($NaBH_4$) = 1280 cm^{-1}) > (ν_2 (KBH_4) = 1240 cm^{-1}) and (ν_1 ($NaBH_4$) = 2325 cm^{-1}) > (ν_1 (KBH_4) = 2305 cm^{-1}), whereas the melting temperature (T_m) varies in the opposite direction, T_m ($LiBH_4$) < T_m ($NaBH_4$) < T_m (KBH_4). The value of ν_1 of $LiBH_4$ was reported at 2293 cm^{-1} and did not follow the relation due to the difference of the crystal system. $LiBH_4$ adopts an orthorhombic structure (space group Pcmn) at room temperature, whereas the other alkali metal (Na, K, Rb and Cs) borohydrides crystallize in a rock salt, face-centered-cubic structure. According to the ATR spectra of Renaudin et al. [32], ν_3 is found to decrease in the order $NaBH_4$ > KBH_4 > $RbBH_4$ > $CsBH_4$. This indicates an inverse correlation between T_d of the borohydride and ν_3 of BH_4^- anion. Based on these results, it can be said that in a given X-group where A is changing, an increase of ν_3(i-BH_4^-) would be accompanied with a decrease of T_d. At the same time, a_0 (AX), R (AX), I_c (AX) and -ΔH (AX) decrease.

DSC data reveal stabilization with increasing chloride-substitution of $NaBH_4$ [28]. Sieverts measurements of the hexagonal $Li(BH_4)_{0.5}Br_{0.5}$ indicate similar H_2 release as for the unsubstituted pattern $LiBH_4$ [29]. This indicates that the substitution, with a more electronegative anion, localizes the negative charge on the B-H bond, stabilizing, thus, the borohydride. Therefore, it could be deduced that for the A-series where the anionic element X is varying, an increase of ν_3(i-BH_4^-) is accompanied with an increase of T_d. At the same time, a_0 (AX) decreases, R (AX), I_c (AX) and -Δ_fH (AX) are increased. Further experiments are still needed to demonstrate the role of the electronegativity of the anion and the thermal stability of the borohydride.

3.3. BH_4-Frequency Variations Dependences on Fundamental Parameter Sets in DFT

The experimental IR frequencies of i-BH_4^- in NaX (Cl, Br, I) are shown in Figure 7a as a function of the lattice parameter a_0 of the halides: ν_4 is represented by 2*ν_4 and obtained by simply doubling the values of ν_4 (* denotes the multiplication), together with the three other peaks, namely $2\nu_{4F-}$ and ν_{3F+} (the subscript $_{F-}$ and $_{F+}$ are used to denote the Fermi resonance effect) and the combination mode $\nu_2 + \nu_4$. Values given by Renaudin et al. [32] for compositions MBH_4, M = N, K, Rb, Cs are also included for comparison (the values are taken as obtained by ATR-method for $2\nu_{4F-}$ and ν_{3F+} and $\nu_2 + \nu_4$; for 2*ν_4 we used the Raman values of ν_4). All frequencies increase with decreasing lattice parameter as discussed above. It is observed that the frequency-dependence on the lattice parameter is weaker for MBH_4 compared to i-BH_4^- in NaX. The overtone frequency 2*ν_4 comes in all cases well between $2\nu_{4F-}$ and ν_{3F+}. This visualizes the Fermi resonance effect characteristic of the BH_4^- anion which occurs between ν_3 and the overtone and combination modes. The Fermi resonance observed in the Raman and IR spectra of the tetrahedral BH_4^- occurs between the stretching and overtone and combination modes and redistributes the intensities and changes the frequencies [35,36]. As a result, the overtone $2\nu_4$ and combination $\nu_2 + \nu_4$ modes appear with much greater intensity than would have been expected and the IR frequencies are shifted from the values at which they would otherwise have appeared ($2\nu4F- < 2^*\nu_4 < \nu_{3F+}$).

The same trends are obtained from DFT calculations at generalized gradient approximation (GGA) level (Figure 7b). It has to be noted that the calculations could not be completed for i-BH_4^- directly, i.e., in the highly diluted limit. Instead the calculations were carried out for compositions $Na(BH_4)_{0.25}X_{0.75}$ with X = Cl, Br, I. The Fermi resonance effect cannot be considered since CRYSTAL does not allow for incorporation of anharmonic effects. Thus, simple approximations of overtones and combination bands had to be made. Therefore, the theoretical values for 2 × ν_4 and ν_3, as well as the combination mode $\nu_2 + \nu_4$ (by simple addition of the harmonic values) are shown related on the lattice parameter values as obtained with DFT. A quasi-linear relationship between lattice parameter and composition $Na(BH_4)_{1-x}X_x$ with x = 0, 0.25, 0.5, 1 and X = Cl, Br or I, was obtained, where the parameter values are in excellent agreement with experiment for the endmembers. Moreover, the frequency variation dependent on lattice parameter is more pronounced for

NaX, X = Cl, Br, I, compared to the series MBH_4 with M = Na, K, Rb, Cs. The absolute values of calculated and measured frequencies and lattice parameters are close. Different from the expectations, the theoretically optimized structures show only slight variations in B–H bond distances. The changes are about one order of magnitude smaller compared to the data given by Renaudin et al. [32]. Rather small variation were also obtained by others using ab initio methods [58]. We therefore conclude that the B–H bond variation is not responsible for the observed frequency changes, but rather the long-distance tail of the B–H potential which is affected by the nearest and next-nearest neighbors.

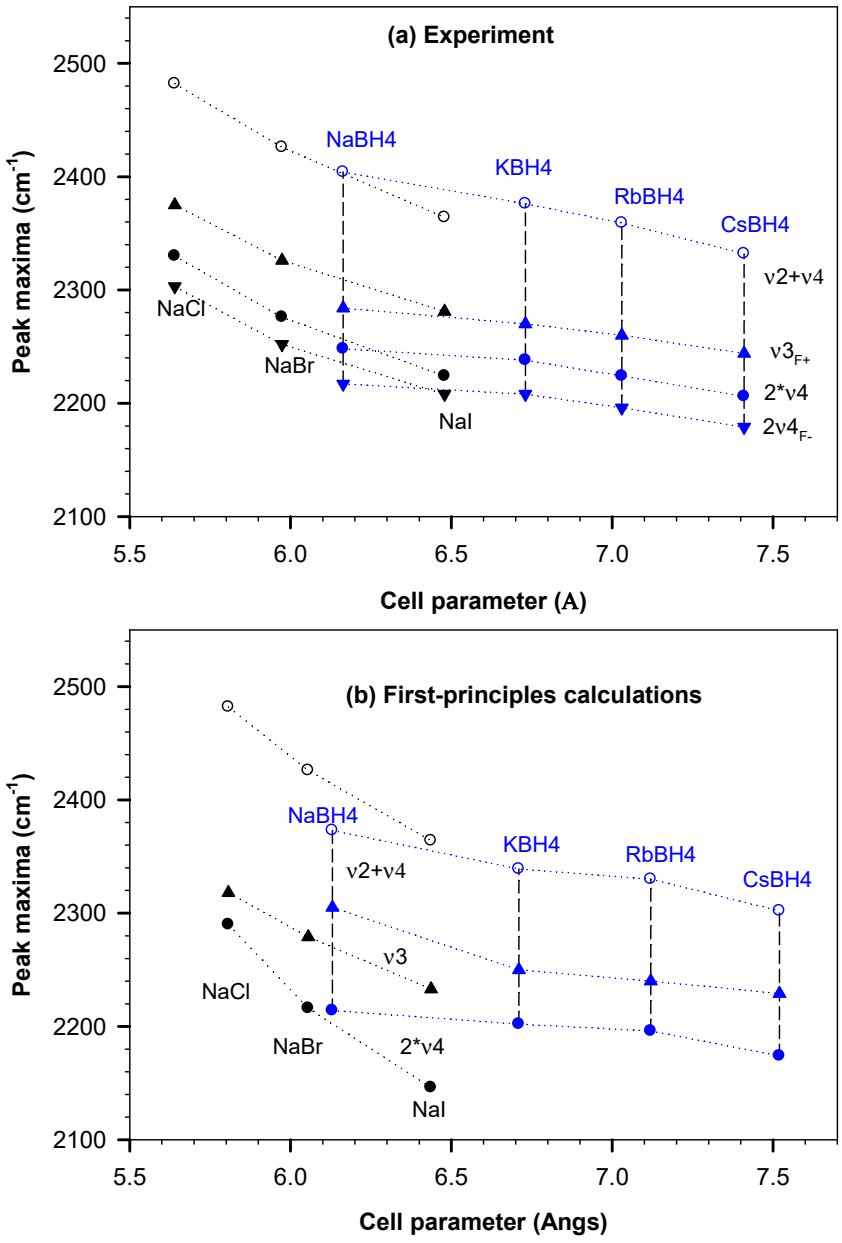

Figure 7. (**a**) Experimental peak positions of ν_4 expressed in the term of $2^*\nu_4$, $2\nu_{4F-}$, ν_{3F+} ($_{F-}$, $_{F+}$ denotes the Fermi−resonance effect) and $\nu_2 + \nu_4$ of i-BH_4^- in NaX, X = Cl, Br, I and MBH_4 (taken from Renaudin et al. [32]) as a function of the cell parameter a_0. (**b**) Calculated (first principles) peak positions of BH_4^- anion in $Na(BH_4)_{0.25}X_{0.75}$ with X = Cl, Br, I and MBH_4, M = Na, K, Rb, Cs as a function of calculated unit cell parameters.

4. Conclusions

The nearest-neighbor coordination has significant influence on the B–H bonding strength of the BH_4^- anion predicting the variation of the IR frequencies in different halides. The BH_4^- anion isolated in AX crystal (i-BH_4^-/AX) yields very sharp IR absorption bands. The IR frequencies of i-BH_4^- are found to depend on the nature of the AX matrix. Systematic variations are observed between the asymmetrical stretching ν_3(i-BH_4^-) and different structural parameters of AX. The correlations established are applicable to homologous series of AX possessing the same cationic A element (A-series: Na-, K-, Rb-series) or the same anionic X element (X-series: Cl-, Br and I-series). For example, when the cationic element A of AX is kept constant for the A-series of AX (A-series: Na-, K- and Rb-series), ν_3(i-BH_4^-) decreases linearly with increasing cell parameter a_0 of AX. A similar quasi-linear trend is observed for the respective anionic X-series. The correlation between ν_3(i-BH_4^-) and a_0(AX) for the homologous series is almost linear and can be written as ν_3(i-BH_4^-) = $\alpha.a_0$ (AX) + β. The absolute value of the slope decreases when increasing the ionic radii of the cation A or the anion X of A-groups and X-groups, respectively. Moreover, higher values are obtained for the A-groups compared to the X-groups. This indicates that smaller cations and anions produces deeper changes in ν_3(i-BH_4^-) and that ν_3(i-BH_4^-) is strongly affected by the nature of X rather than A. The correlation study on the ν_3(i-BH_4^-) is extended in terms of the ratio of the effective ionic radius of the cation to the ionic radius of the anion ($R = r_A/r_X$), the Pauling electronegativity (χ_P) of A and X, respectively, the ionic character (I_c) and the standard enthalpy of formation of AX ($\Delta_f H$). An approximately linear relationship is observed between ν_3(i-BH_4^-) and the contribution of the short-range interactions energies of AX pointing the strong impact of the repulsive forces between BH_4^- and its nearest neighbors on ν_3(i-BH_4^-). DFT calculations obtain a reasonable agreement with experimental values, without showing significant variations of the B–H bond length.

Author Contributions: Investigation, Z.A., A.G.S., A.C.U., T.B. and C.H.R.; Methodology, Z.A., A.G.S., A.C.U., T.B. and C.H.R.; Writing—Review & Editing, Z.A., A.G.S., A.C.U., T.B. and C.H.R. All authors have read and agreed to the published version of the manuscript.

Funding: ZA was funded by DAAD Ref 441: A/10/97515. CHR used LUH-internal support and RU764/6-1, AGS and ACU were funded within the DFG project of BR1768/8-1.

Institutional Review Board Statement: Not applicable.

Informed Consent Statement: Not applicable.

Data Availability Statement: Data obtained as described.

Conflicts of Interest: The authors declare no conflict of interest.

References

1. Züttel, A.; Borgschulte, A.; Orimo, S.I. Tetrahydroborates as new hydrogen storage materials. *Scr. Mater.* **2007**, *56*, 823–828. [CrossRef]
2. Schlesinger, H.I.; Brown, H.C.; Finholt, A.E.; Gilbreath, J.R.; Hoekstra, H.R.; Hyde, E.K. Sodium Borohydride, Its Hydrolysis and its Use as a Reducing Agent and in the Generation of Hydrogen. *J. Am. Chem. Soc.* **1953**, *75*, 215–219. [CrossRef]
3. Demirci, U.B.; Akdim, O.; Andrieux, J.; Hannauer, J.; Chamoun, R.; Miele, P. Sodium borohydride hydrolysis as hydrogen generator: Issues, state of the art and applicability upstream froma fuel cell. *Fuel Cells* **2010**, *10*, 335–350. [CrossRef]
4. Urgnani, J.; Torres, F.J.; Palumbo, M.; Baricco, M. Hydrogen release from solid state $NaBH_4$. *Int. J. Hydrogen Energy* **2008**, *33*, 3111–3115. [CrossRef]
5. Mao, J.; Guo, Z.; Nevirkovets, I.P.; Liu, H.K.; Dou, S.X. Hydrogen De-/absorption improvement of $NaBH_4$ catalyzed by titanium-based additives. *J. Phys. Chem. C* **2012**, *116*, 1596–1604. [CrossRef]
6. Humphries, T.D.; Kalantzopoulos, G.N.; Llamas-Jansa, I.; Olsen, J.E.; Hauback, B.C. Reversible hydrogenation studies of $NaBH_4$ milled with Ni-containing additives. *J. Phys. Chem. C* **2013**, *117*, 6060–6065. [CrossRef]
7. Ngene, P.; Van Den Berg, R.; Verkuijlen, M.H.W.; De Jong, K.P.; De Jongh, P.E. Reversibility of the hydrogen desorption from $NaBH_4$ by confinement in nanoporous carbon. *Energy Environ. Sci.* **2011**, *4*, 4108–4115. [CrossRef]
8. Peru, F.; Garroni, S.; Campesi, R.; Milanese, C.; Marini, A.; Pellicer, E.; Baro, M.D.; Mulas, G. Ammonia-free infiltration of $NaBH_4$ into highly-ordered mesoporous silica and carbon matrices for hydrogen storage. *J. Alloys Compd.* **2013**, *580*, S309–S312. [CrossRef]

9. Zhang, L.; Xiao, X.; Fan, X.; Li, S.; Ge, H.; Wang, Q.; Chen, L. Fast hydrogen release under moderate conditions from $NaBH_4$ destabilized by fluorographite. *RSC Adv.* **2014**, *4*, 2550–2556. [CrossRef]
10. Rude, L.H.; Filsø, U.; D'Anna, V.; Spyratou, A.; Richter, B.; Hino, S.; Jensen, T.R. Hydrogen-fluorine exchange in $NaBH_4$-$NaBF_4$. *Phys. Chem. Chem. Phys.* **2013**, *15*, 18185–18194. [CrossRef] [PubMed]
11. Zhang, Z.G.; Wang, H.; Zhu, M. Hydrogen release from sodium borohydrides at low temperature by the addition of zinc fluoride. *Int. J. Hydrogen Energy* **2011**, *36*, 8203–8208. [CrossRef]
12. Buhl, J.C.; Gesing, T.M.; Rüscher, C.H. Synthesis, crystal structure and thermal stability of tetrahydroborate sodalite $Na_8[AlSiO_4]_6(BH_4)_2$. *Microporous Mesoporous Mater.* **2005**, *80*, 57–63. [CrossRef]
13. Buhl, J.C.; Schomborg, L.; Rüscher, C.H. Enclosure of Sodium Tetrahydroborate ($NaBH_4$) in Solidified Aluminosilicate Gels and Microporous Crystalline Solids for Fuel Processing. In *Hydrogen Storage*; InTechOpen: London, UK, 2012.
14. Rüscher, C.H. Boronhydride-geopolymer composites. *J. Ceram. Sci. Technol.* **2017**, *8*, 399–410. [CrossRef]
15. Schneider, A.G.; Bredow, T.; Schomborg, L.; Rscher, C.H. Structure and IR vibrational spectra of $Na_8[AlSiO_4]_6(BH_4)_2$: Comparison of theory and experiment. *J. Phys. Chem. A* **2014**, *118*, 7066–7073. [CrossRef]
16. Rüscher, C.H.; Schomborg, L.; Bredow, T. Experiments on the thermal activation of hydrogen release of $NaBH_4$-sodalites characterized by IR- and MAS-NMR spectroscopy. *Int. J. Hydrogen Energy* **2022**. *under review*.
17. Mesmer, R.E.; Jolly, W.L. The Hydrolysis of Aqueous Hydroborate. *Inorg. Chem.* **1962**, *1*, 608–612. [CrossRef]
18. Kreevoy, M.M.; Hutchins, J.E.C. H_2BH_3 as an Intermediate in Tetrahydridoborate Hydrolysis. *J. Am. Chem. Soc.* **1972**, *94*, 6371–6376. [CrossRef]
19. Nakamori, Y.; Miwa, K.; Ninomiya, A.; Li, H.; Ohba, N.; Towata, S.I.; Orimo, S.I. Correlation between thermodynamical stabilities of metal borohydrides and cation electronegativites: First-principles calculations and experiments. *Phys. Rev. B—Condens. Matter Mater. Phys.* **2006**, *74*, 1–9. [CrossRef]
20. Nakamori, Y.; Li, H.W.; Kikuchi, K.; Aoki, M.; Miwa, K.; Towata, S.I.; Orimo, S.I. Thermodynamical stabilities of metal-borohydrides. *J. Alloys Compd.* **2007**, *446–447*, 296–300. [CrossRef]
21. Matsunaga, T.; Buchter, F.; Miwa, K.; Towata, S.; Orimo, S.; Züttel, A. Magnesium borohydride: A new hydrogen storage material. *Renew. Energy* **2008**, *33*, 193–196. [CrossRef]
22. Graetz, J. New approaches to hydrogen storage. *Chem. Soc. Rev.* **2009**, *38*, 73–82. [CrossRef] [PubMed]
23. Hinze, J. The concept of electronegativity of atoms in molecules. *Theor. Comput. Chem.* **1999**, *6*, 189–212. [CrossRef]
24. Ravnsbæk, D.; Filinchuk, Y.; Cerenius, Y.; Jakobsen, H.J.; Besenbacher, F.; Skibsted, J.; Jensen, T.R. A Series of Mixed-Metal Borohydrides. *Angew. Chem.* **2009**, *121*, 6787–6791. [CrossRef]
25. Brinks, H.W.; Fossdal, A.; Hauback, B.C. Adjustment of the stability of complex hydrides by anion substitution. *J. Phys. Chem. C* **2008**, *112*, 5658–5661. [CrossRef]
26. Yin, L.; Wang, P.; Fang, Z.; Cheng, H. Thermodynamically tuning $LiBH_4$ by fluorine anion doping for hydrogen storage: A density functional study. *Chem. Phys. Lett.* **2008**, *450*, 318–321. [CrossRef]
27. Ravnsbæk, D.B.; Rude, L.H.; Jensen, T.R. Chloride substitution in sodium borohydride. *J. Solid State Chem.* **2011**, *184*, 1858–1866. [CrossRef]
28. Olsen, J.E.; Sørby, M.H.; Hauback, B.C. Chloride-substitution in sodium borohydride. *J. Alloys Compd.* **2011**, *509*, L228–L231. [CrossRef]
29. Rude, L.H.; Zavorotynska, O.; Arnbjerg, L.M.; Ravnsbæk, D.B.; Malmkjær, R.A.; Grove, H.; Jensen, T.R. Bromide substitution in lithium borohydride, LiBH4-LiBr. *Int. J. Hydrogen Energy* **2011**, *36*, 15664–15672. [CrossRef]
30. Rude, L.H.; Groppo, E.; Arnbjerg, L.M.; Ravnsbaek, D.B.; Malmkjaer, R.A.; Filinchuk, Y.; Jensen, T.R. Iodide substitution in lithium borohydride, $LiBH_4$-LiI. *J. Alloys Compd.* **2011**, *509*, 8299–8305. [CrossRef]
31. Vajeeston, P.; Ravindran, P.; Kjekshus, A.; Fjellvåg, H. Structural stability of alkali boron tetrahydrides ABH_4 (A=Li, Na, K, Rb, Cs) from first principle calculation. *J. Alloys Compd.* **2005**, *387*, 97–104. [CrossRef]
32. Renaudin, G.; Gomes, S.; Hagemann, H.; Keller, L.; Yvon, K. Structural and spectroscopic studies on the alkali borohydrides MBH_4 (M = Na, K, Rb, Cs). *J. Alloys Compd.* **2004**, *375*, 98–106. [CrossRef]
33. Harvey, K.B.; McQuaker, N.R. Infrared and Raman Spectra of Potassium and Sodium Borohydride. *Can. J. Chem.* **1971**, *49*, 3272–3281. [CrossRef]
34. Heyns, A.M.; Schutte, C.J.H.; Scheuermann, W. Low-temperature infrared studies. IX. The infrared and Raman spectra of sodium d4-borohydride $NaBD_4$. *J. Mol. Struct.* **1971**, *9*, 271–281. [CrossRef]
35. Memon, M.I.; Wilkinson, G.R.; Sherman, W.F. Vibrational studies of BH_4- and BD_4- isolated in alkali halides. *J. Mol. Struct.* **1982**, *80*, 113–116. [CrossRef]
36. Memon, M.I.; Sherman, W.F.; Wilkinson, G.R. Fermi resonances in the Raman spectra of alkali halide/BH_4-. *J. Mol. Struct.* **1984**, *115*, 213–216. [CrossRef]
37. Dovesi, R.; Orlando, R.; Civalleri, B.; Roetti, C.; Saunders, V.R.; Zicovich-Wilson, C.M. CRYSTAL: A computational tool for the ab initio study of the electronic properties of crystals. *Z. Für. Krist.–Cryst. Mater.* **2005**, *220*, 571–573. [CrossRef]
38. Dovesi, R.; Roberto, O.; Alessandro, E.; Claudio, M.Z.-W.; Bartolomeo, C.; Silvia, C.; Lorenzo, M.; Matteo, F.; Marco, D.L.P.; Philippe, D.; et al. *CRYSTAL14 User's Manual*; University of Turin: Torino, Italy, 2014; p. 382.
39. Perdew, J.P.; Yue, W. Accurate and simple density functional for the electronic exchange energy: Generalized gradient approximation. *Phys. Rev. B Condens. Matter* **1986**, *33*, 8800–8802. [CrossRef]

40. Dovesi, R.; Roetti, C.; Freyria-Fava, C.; Prencipe, M.; Saunders, V.R. On the elastic properties of lithium, sodium and potassium oxide. An ab initio study. *Chem. Phys.* **1991**, *156*, 11–19. [CrossRef]
41. Leininger, T.; Nicklass, A.; Küchle, W.; Stoll, H.; Dolg, M.; Bergner, A. The accuracy of the pseudopotential approximation: Non-frozen-core effects for spectroscopic constants of alkali fluorides XF (X = K, Rb, Cs). *Chem. Phys. Lett.* **1996**, *255*, 274–280. [CrossRef]
42. Dovesi, R.; Ermondi, C.; Ferrero, E.; Pisani, C.; Roetti, C. Hartree-Fock study of lithium hydride with the use of a polarizable basis set. *Phys. Rev. B* **1984**, *29*, 3591–3600. [CrossRef]
43. Orlando, R.; Dovesi, R.; Roetti, C.; Saunders, V.R. Ab initio Hartree-Fock calculations for periodic compounds: Application to semiconductors. *J. Phys. Condens. Matter* **1990**, *2*, 7769–7789. [CrossRef]
44. Apra, E.; Causa, M.; Prencipe, M.; Dovesi, R.; Saunders, V.R. On the structural properties of {NaCl}: An ab initio study of the B1-B2 phase transition. *J. Phys. Condens. Matter* **1993**, *5*, 2969–2976. [CrossRef]
45. Peintinger, M.F.; Oliveira, D.V.; Bredow, T. Consistent Gaussian basis sets of triple-zeta valence with polarization quality for solid-state calculations. *J. Comput. Chem.* **2013**, *34*, 451–459. [CrossRef] [PubMed]
46. Stoll, H.; Metz, B.; Dolg, M. Relativistic energy-consistent pseudopotentials–recent developments. *J. Comput. Chem.* **2002**, *23*, 767–778. [CrossRef] [PubMed]
47. The Inorganic Crystal Structure Database (ICSD). Available online: https://icsd.products.fiz-karlsruhe.de/ (accessed on 9 March 2022).
48. Hanson, R.M. Jmol—A paradigm shift in crystallographic visualization. *J. Appl. Crystallogr.* **2010**, *43*, 1250–1260. [CrossRef]
49. Hisatsune, I.C.; Suarez, N.H. Infrared Spectra of Metaborate Monomer and Trimer Ions. *Inorg. Chem.* **1964**, *3*, 168–174. [CrossRef]
50. Ketelaar, J.A.A.; Schutte, C.J.H. The borohydride ion (BH_4^-) in a face-centred cubic alkali-halide lattice. *Spectrochim. Acta* **1961**, *17*, 1240–1243. [CrossRef]
51. Nasar, A. Correlation between standard enthalpy of formation, structural parameters and ionicity for alkali halides. *J. Serb. Chem. Soc.* **2013**, *78*, 241–253. [CrossRef]
52. Bryant, J.I.; Turrell, G.C. Infrared Spectra of the Azide Ion in Alkali-Halide Lattices. *J. Chem. Phys.* **1962**, *37*, 1069–1077. [CrossRef]
53. Sherman, W.F.; Wilkinson, G.R. Infrared and raman studies on the vibrational spectra of impurities in ionic and covalent crystals. In *Vibrational Spectroscopy of Trapped Species*; Wiley: London, UK, 1973; p. 291.
54. Field, G.R.; Sherman, W.F. Cyanide ion—Environmental perturbation of its vibrational and rotational motion when isolated in alkali halides. *J. Chem. Phys.* **1967**, *47*, 2378–2389. [CrossRef]
55. Strasheim, A.; Buijs, K. Infrared absorption of nitrate ions dissolved in solid alkali halides. *J. Chem. Phys.* **1961**, *34*, 691–692. [CrossRef]
56. Seitz, F. *The Modern Theory of Solids*; McGraw-Hill Book Company, Incorporated: New York, NY, USA, 1940.
57. Orimo, S.; Nakamori, Y.; Züttel, A. Material properties of MBH_4 (M = Li, Na, and K). *Mater. Sci. Eng. B Solid-State Mater. Adv. Technol.* **2004**, *108*, 51–53. [CrossRef]
58. Zhang, X.D.; Hou, Z.F.; Jiang, Z.Y.; Hou, Y.Q. Elastic properties of MBH_4 (M = Na, K, Rb, Cs). *Phys. B Condens. Matter* **2011**, *406*, 2196–2199. [CrossRef]